

Article

Synthesis and Pharmacological Characterization of New Photocaged Agonists for Histamine H₃ and H₄ Receptors

Yang Zheng [†], Meichun Gao [†], Maikel Wijtmans , Henry F. Vischer  and Rob Leurs ^{*}

Division of Medicinal Chemistry, Faculty of Science, Amsterdam Institute of Molecular and Life Sciences, Vrije Universiteit Amsterdam, 1081 HZ Amsterdam, The Netherlands; y.zheng@vu.nl (Y.Z.); m.c.gao@vu.nl (M.G.); m.wijtmans@vu.nl (M.W.); h.f.vischer@vu.nl (H.F.V.)

* Correspondence: r.leurs@vu.nl

[†] These authors contributed equally to this work.

Abstract: The modulation of biological processes with light-sensitive chemical probes promises precise temporal and spatial control. Yet, the design and synthesis of suitable probes is a challenge for medicinal chemists. This article introduces a photocaging strategy designed to modulate the pharmacology of histamine H₃ receptors (H₃R) and H₄ receptors (H₄R). Employing the photoremovable group BODIPY as the caging entity for two agonist scaffolds—immepip and 4-methylhistamine—for H₃R and H₄R, respectively, we synthesized two BODIPY-caged compounds, **5** (VUF25657) and **6** (VUF25678), demonstrating 10–100-fold reduction in affinity for their respective receptors. Notably, the caged H₃R agonist, VUF25657, exhibits approximately a 100-fold reduction in functional activity. The photo-uncaging of VUF25657 at 560 nm resulted in the release of immepip, thereby restoring binding affinity and potency in functional assays. This approach presents a promising method to achieve optical control of H₃R receptor pharmacology.

Keywords: photocaging; BODIPY cage; histamine; H₃ receptor; H₄ receptor



Citation: Zheng, Y.; Gao, M.; Wijtmans, M.; Vischer, H.F.; Leurs, R. Synthesis and Pharmacological Characterization of New Photocaged Agonists for Histamine H₃ and H₄ Receptors. *Pharmaceuticals* **2024**, *17*, 536. <https://doi.org/10.3390/ph17040536>

Academic Editor: Honorina Cidade

Received: 25 March 2024

Revised: 18 April 2024

Accepted: 19 April 2024

Published: 21 April 2024



Copyright: © 2024 by the authors. Licensee MDPI, Basel, Switzerland. This article is an open access article distributed under the terms and conditions of the Creative Commons Attribution (CC BY) license (<https://creativecommons.org/licenses/by/4.0/>).

1. Introduction

Photopharmacology represents a new and cutting-edge area in the field of chemical biology, offering precise spatiotemporal control over biological processes [1–4]. Photopharmacology involves the use of light to modulate the activity of bioactive compounds, providing a non-invasive means to influence cellular functions with high precision [1–4]. Photocaging is one of the important strategies employed in the field of photopharmacology and this approach involves the temporary inactivation of a bioactive molecule through a light-sensitive protecting group [5–8]. Upon exposure to light, the caging group is removed, releasing the bioactive molecule to act on its respective target. This approach holds great potential for studying and modulating cellular signaling pathways, potentially offering unprecedented spatial and temporal control of receptor activation.

In this study, we report our efforts in the field of photopharmacology of G protein-coupled receptors (GPCR) by developing photocaged agonists specifically tailored for histamine H₃- and H₄ receptors (H₃R and H₄R). The H₃R and H₄R are G α_i -coupled GPCRs and integral components of the histaminergic system [9,10]. Both GPCRs play a pivotal role in regulating various physiological processes and are emerging as promising targets for therapeutic intervention [9,10]. The H₃R is primarily localized in the central nervous system, modulating the release of neurotransmitters such as histamine, dopamine, and acetylcholine. The intricate involvement of the H₃R in cognitive functions, sleep-wake cycles, and appetite regulation underscores its significance as a potential target for neurological and psychiatric disorders [11–13]. Moreover, recently an H₃R inverse agonist/antagonist (pitolisant) was approved for therapeutic use in narcolepsy (Wakix[®]) or in apnea patients suffering from excessive daytime sleepiness (Ozawade[®]) [14–16]. On the other hand, the H₄R, although more recently discovered, has sparked considerable

interest due to its expression in the immune system [9,10]. As an immune modulator, the H₄R is implicated in the regulation of inflammatory responses, making it an attractive target for conditions involving immune dysregulation, such as allergies and autoimmune diseases [17,18]. Recently, its role in neurological disorders has also gained attention [19].

To allow spatio-temporal studies of the function of H₃R and H₄R, we focused on the design, synthesis, and characterization of novel photocaged agonists to enable spatiotemporal control of histamine receptor activity. Previously, caging groups such as nitrobenzyl, coumarin, and BODIPY (boron-dipyrromethene) have been successfully employed in the field of photocaging [2,6–8,20]. Especially, BODIPY dyes have gained interest as caging groups in view of their photostability and strong absorbance in the visible region [21]. This last property makes BODIPY compounds well-suited for light-triggered applications in biological context, as UV (ultraviolet) light is well-known to damage biomolecules. In this study, we report on the synthesis and characterization of BODIPY-caged immapip and 4-methylhistamine, two small molecule agonists known to act on H₃R and H₄R [22,23]. Caged compounds were analyzed for their photochemical properties, aggregation, and molecular pharmacological properties in radioligand binding and GPCR signaling studies.

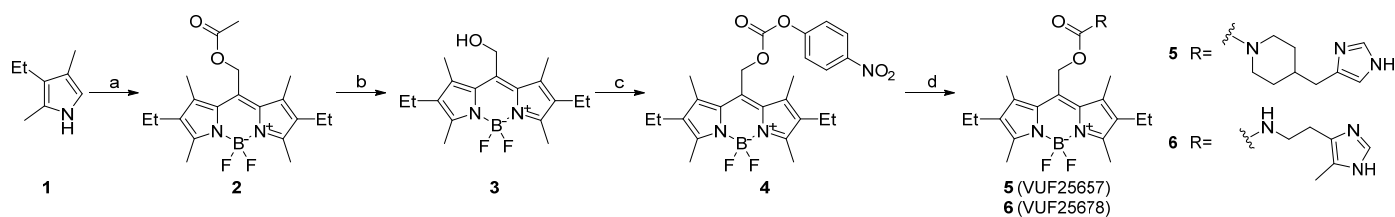
2. Results

2.1. Design, Synthesis, and Photochemical Characterization of Photocaged Compounds

Following the discovery of immapip as a potent H₃R agonist, various modifications have been reported in structure–activity relationship (SAR) studies. Among those, three earlier described modifications were instrumental in the design of photocaged immapip. First, the introduction of bulky N-alkyl substituents, such as an isopropyl group on the piperidine ring, by Kitbunnadaj et al. results in a remarkable >100-fold decrease in affinity [24]. Next, N-phenyl piperidine substituted immapip analogs prepared by Ishikawa et al. showed a pK_i range of 1–60 nM, representing 3 to 200-fold lower activity compared to immapip [25]. Lastly, the investigation by Vaccaro et al. of the basicity of the piperidine nitrogen revealed that analogs with a carbonyl group were 10 to >1500-fold less active towards H₃R [26]. In contrast, so far very few immapip analogs with substituents on the imidazole N-atom have been reported [26]. Thus, in the design of our BODIPY-based photocaged H₃R agonist, we considered photocaging of the piperidine amine functional group as the most viable approach.

In contrast to H₃R agonists, there are significantly fewer reported H₄R agonists, and many of them also exhibit activity towards H₃R. In 2005, 4-methylhistamine was reported as a selective H₄R agonist over H₃R [22], making it an ideal candidate for the design of a photocaged H₄R agonist. Within the structure of 4-methylhistamine, there are two potential positions for the introduction of the photocage group (the amino and imidazole groups). However, SARs of these two positions have not been well explored. We opted for attaching the required carbamate to the amino group rather than to the imidazole in view of its anticipated higher stability in the dark. Indeed, the recently published cryo-EM structures of histamine-bound H₄R [27,28] indicate that the primary amino group of histamine directly or indirectly forms a salt bridge with Asp^{943.32} in transmembrane domain 3 and thus holds promise as a site for photocaging. From the three main classes of photocages in the literature, BODIPY was chosen in this study as photocaging group for the H₃R/H₄R ligands due to its lower-energy and rapid uncaging compared with o-nitrobenzyl and coumarin cages [29–31].

The synthesis of the BODIPY scaffold (Scheme 1) starts with pyrrole 1 [32–35]. By reacting this precursor with 2-chloro-2-oxoethyl acetate, followed by the addition of boron trifluoride diethyl etherate, 2 was obtained in a moderate yield. Subsequent hydrolysis provided alcohol 3. By reacting alcohol 3 with 4-nitrophenyl chloroformate, key intermediate 4 was obtained in a high yield. BODIPY-caged analogs 5 (VUF25657) and 6 (VUF25678) were prepared from 4 by a substitution reaction with immapip and 4-methylhistamine, respectively.



Scheme 1. (a) (i) 2-chloro-2-oxoethyl acetate, DCM, reflux, 24 h; (ii) BF₃·O(C₂H₅)₂, TEA, rt, 30 min, 22%; (b) NaOH (aq.), MeOH, DCM, rt, 3 h, 42%; (c) 4-NO₂PhOCOCl, pyridine, toluene, rt, 3 h, 87%; (d) R₁NHR₂, DIPEA, THF, rt, 4 h, 22% for 5 and 55% for 6.

Next, the photochemical properties of the caged VUF25657 and VUF25678 were investigated. Due to the large conjugation system of the BODIPY cage, the aqueous solubility of two caged compounds is limited to 3.2 μM, as determined by the nephelometry measurements (Figure S1). Based on the photochemical stability results in Figure S2, photo characterizations of VUF25657 and VUF25678 were performed under red LED light. Due to the low absorbance of immpip and 4-methylhistamine at 230 and 254 nm, a quantitative analysis method based on mass (MS) detection was employed. First, calibration curves of monitored compounds with the corresponding reference compound of the same molecular weight were built (Figure S3). Then, after illumination, the reference compounds were added to LCMS samples as internal standards. Based on the MS signal areas, the concentrations of caged compounds and parent compounds could be monitored. In Tris-HCl buffer (50 mM, pH 7.4), the absorption maximum (λ_{max}) was determined to be 551 nm for VUF25657 (Figure 1A) and 546 nm for VUF25678 (Figure S4A). Within 20 min of continuous illumination of VUF25657 at 3.2 μM in Tris-HCl buffer with 560 ± 5 nm, the absorption centered around 550 nm decreased significantly (Figure 1A), and the active ligand immpip could be obtained (Figure 1B). The same results were observed for caged-4-methylhistamine (VUF25678) (Figure S4). After 180 s of illumination, the concentration of immpip reached 0.92 μM, amounting to 29% uncaging efficiency. Further illumination led to a decreased immpip concentration (for example, 0.53 μM at 20 min). One potential explanation for this could be the reaction of immpip with side products or intermediates formed during the uncaging process. A similar uncaging profile was observed for VUF25678 (Figure S4B).

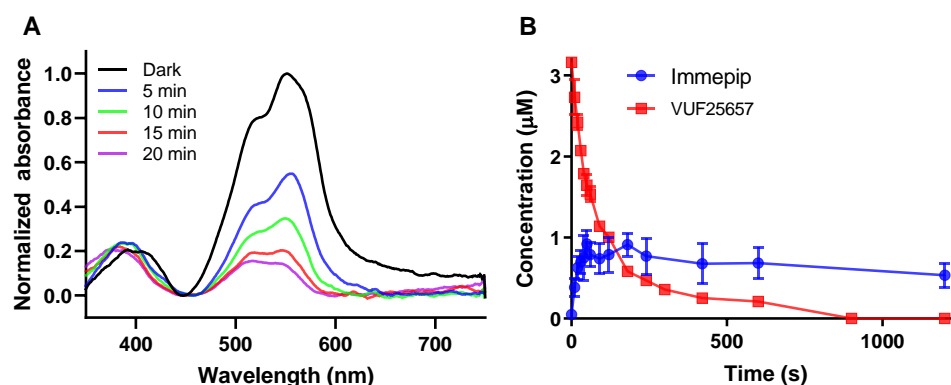


Figure 1. Photo-uncaging followed by UV-Vis (ultraviolet-visible) and LC-MS analysis. (A) VUF25657 (3.2 μM) was illuminated under 560 nm in Tris-HCl buffer (50 mM, pH 7.4)/1% DMSO at room temperature and a UV-Vis spectrum was measured at intervals. Only the 350–750 nm region is shown; (B) VUF25657 (3.2 μM) was illuminated under green LED light in Tris-HCl buffer (50 mM, pH 7.4)/1% DMSO at 37 °C and LC-MS analysis was performed at different time points using an internal standard.

2.2. Photopharmacological Characterization

The photocaged H₃R and H₄R agonists VUF25657 and VUF25678, either kept in the dark or pre-irradiated at 560 nm to achieve an uncaged state, were evaluated for their

binding affinities by competition binding of the radioligands N- α -[methyl- ^3H] histamine (^3H]NAMH) and ^3H]histamine for the human H_3R and H_4R , respectively. Both GPCRs were transiently expressed in HEK293T cells. Previously, we have shown that ^3H]NAMH and ^3H]histamine saturably bind to the H_3R and H_4R , respectively, with K_D values of 1.37 and 4.40 nM [36]. The parent compounds immapip and 4-methylhistamine (4-MeHA) potently displaced radioligand binding to H_3R (Figure 2A) or H_4R (Figure 2B). Moreover, pre-irradiation of the parent agonist solution at 560 nm did not lead to any difference in affinity (Figure 2A,B). The BODIPY-caged immapip (VUF25657) displayed a 125-fold decreased affinity for H_3R . Illumination of VUF25657 at 560 nm partially restored the observed H_3R affinity, with a 12-fold increase in comparison to its caged state (Table 1). Caging 4-methylhistamine with BODIPY also led to a decreased affinity for H_4R . However, the displacement of radioligand binding by VUF25678 could not be measured at concentrations $> 1 \mu\text{M}$ due to solubility issues. Therefore, the accurate affinity shift between caged and uncaged VUF25678 could not be determined and pharmacological analysis of VUF25678 was halted.

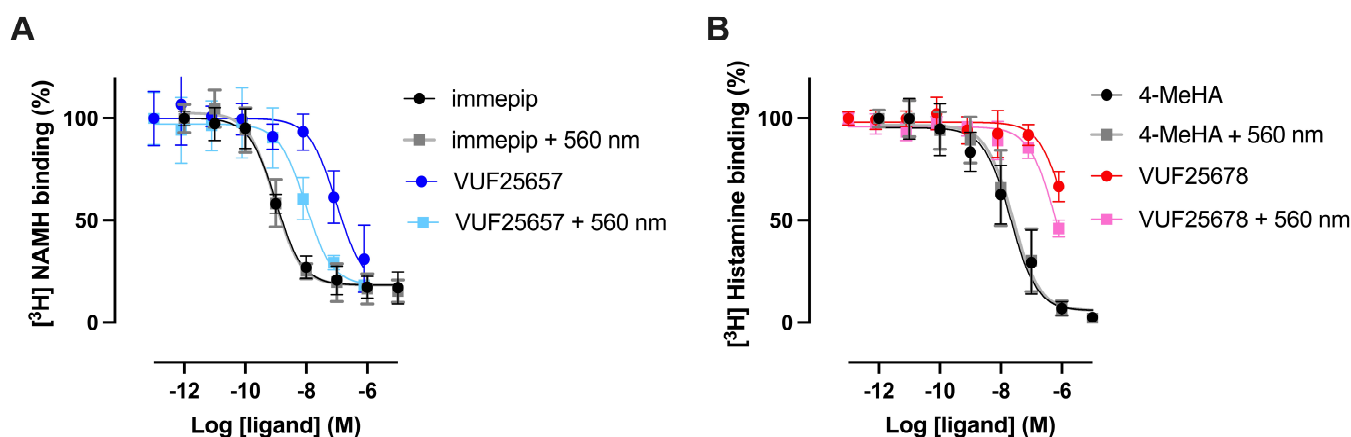


Figure 2. Displacement binding curves of parent, caged, and uncaged ligands for H_3R (A) and H_4R (B). Binding affinities were determined by displacement of the binding of 2 nM ^3H]NAMH and 4 nM ^3H]histamine to H_3R and H_4R , respectively. Caged ligands were either kept in dark or pre-irradiated at 560 nm for 3 min for VUF25657 and 5 min for VUF25678 to achieve the uncaged state. Data shown are mean \pm S.D. from three or four independent experiments, each performed in triplicate.

Table 1. Pharmacological data of photocaged H_3R and H_4R agonist. Statistical difference ($p < 0.05$) of pK_i and pEC_{50} values for the pre-irradiated compound in comparison to that in dark state was determined by unpaired t -test with Welch's and indicated with an asterisk (*). Data are mean \pm S.D. from three or four independent experiments performed in triplicate. N.D. = not determined.

Compound	pK_i		pEC_{50}	
	In Dark	+560 nm	In Dark	+560 nm
VUF25657 (5)	7.3 ± 0.6 (4)	8.4 ± 0.2 (4) *	8.0 ± 0.4 (4)	9.3 ± 0.2 (4) *
immapip	9.4 ± 0.2 (4)	9.4 ± 0.3 (4)	10.5 ± 0.6 (4)	10.2 ± 0.6 (4)
VUF25678 (6)	<6 (3)	<6 (3)	N.D.	N.D.
4-methylhistamine	7.2 ± 0.2 (3)	7.2 ± 0.1 (3)	N.D.	N.D.

Next, the photocaged H_3R agonist VUF25657, which notably displays a significant alteration in binding affinity to H_3R upon irradiation at 560 nm, was further evaluated for its functionality by a FRET-based EPAC cAMP (cyclic adenosine monophosphate) biosensor [37]. H_3R primarily couples to $\text{G}\alpha_i$ protein, which upon activation causes a decrease in intracellular cAMP levels via the inhibition of adenylate cyclase. Therefore, the HEK-EPAC cells were pre-treated with 10 nM of the beta2 adrenergic receptor ($\beta_2\text{AR}$) agonist isoprenaline before H_3R stimulation to enhance the basal intracellular cAMP levels

via β_2 AR- $G\alpha_s$ activation. As anticipated, the H_3R selective agonist immpip reduced the isoprenaline-induced cAMP accumulation, as detected by an increased FRET (fluorescence resonance energy transfer) signal in the EPAC (exchange protein directly activated by cAMP) biosensor (Figure 3A). In line with the binding affinity results, caging immpip with BODIPY (VUF25657) resulted in a decrease potency of cAMP inhibition (316-fold) as compared to immpip. Furthermore, as expected, irradiation of VUF25657 at 560 nm restored the activity for cAMP inhibition, demonstrated a significantly higher potency than its caged state (20-fold) (Figure 3B, Table 1).

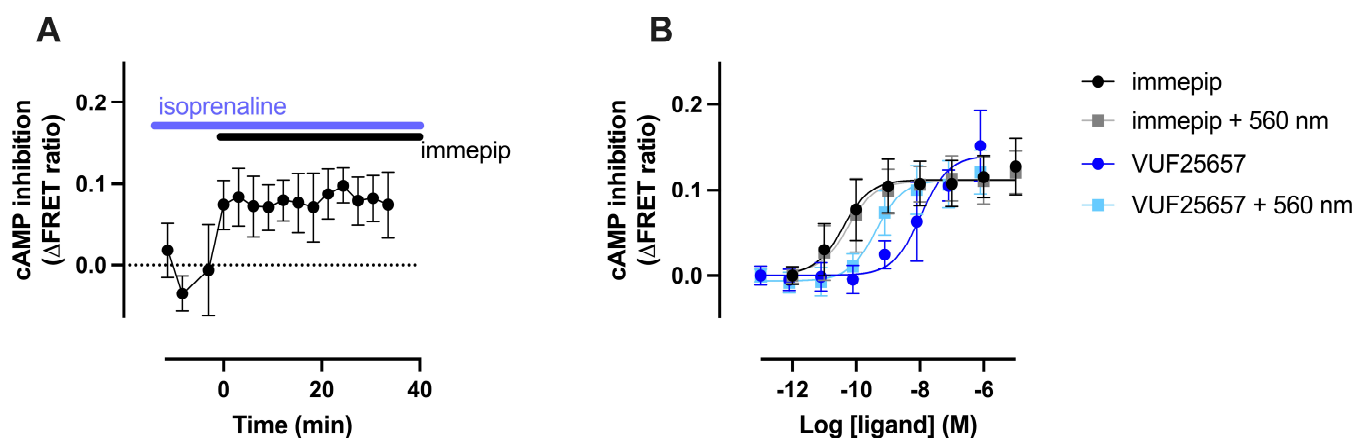


Figure 3. Optical modulation of VUF25657-induced cAMP inhibition in EPAC- H_3R cells. Real time modulation of isoprenaline-induced cAMP accumulation in HEK-EPAC cells by 1 μ M immpip (A). Modulation of isoprenaline-induced cAMP accumulation in HEK-EPAC cells by increasing concentrations of VUF25657 (B). HEK-EPAC cells stably expressing H_3R were pre-stimulated with 10 nM isoprenaline for 10 min before ligand addition. The FRET signal of the EPAC-sensor was measured after 20 min treatment of indicated ligands. VUF25657 was either kept in dark or pre-irradiated at 560 nm for 3 min to release the BODIPY cage. Data are mean \pm S.D. from four independent experiments performed, each in triplicate.

3. Discussion

As an important component of photopharmacology, the photocaging strategy has a long history, compared to the photoswitch strategy, in controlling bioactivity by light. Dating back to the 1980s [38], the photocage strategy had already proven its important role in chemistry, biology, and other related fields [39]. To serve the purpose of spatiotemporal modulation of biological processes, several classes of photocages have been discovered and the concept has been well-developed so far [40]. In this study, the BODIPY cage was successfully coupled to selective H_3R/H_4R agonists and the resulting photocaged ligands could rapidly release the parent agonists. The novel photocaged H_3R ligand VUF25657 was successfully applied in pharmacological assays. This new chemical biology tool exhibits significant activity differences in both H_3R binding affinity and functional H_3R assay before and after uncaging with visible light.

Despite the successful application, certain limitations of the BODIPY cage were also noted in this study. Compared to *o*-nitrobenzyl and coumarin cages, the BODIPY scaffold has a larger conjugation system, resulting in a lower-energy uncaging. However, this larger conjugation system often leads to compounds with low solubility in aqueous environments. The compound concentrations of VUF25657 and VUF25678 in both binding and functional assay had to be limited to maximally 3.2 μ M, as determined by nephelometry. Due to this low concentration and the low absorbance of immpip and 4-methylhistamine at a common UV detection wavelength (such as 254 and 230 nm), a more complex MS-based analytical method than the routine LC-MS was employed to track the uncaging process. In our experiments with the caged H_4R ligand, the release of the parent compound 4-methylhistamine could be monitored. However, due to the low concentration in the experiment and low

activity of 4-methylhistamine, no significant difference was observed in the binding affinity assay before or after irradiation. To improve the aqueous solubility of BODIPY cages, Kand et al. have developed a water-soluble MESNA-BODIPY (2-mercaptoethanesulfonic acid-BODIPY) cage by introducing a sulfonic acid group [41]. However, the applicability of compounds with such a cage may be reduced depending on the target location, as deprotonation might impede the accessibility of their target. Nevertheless, for photocaging of GPCR ligands the future use of water-soluble BODIPY analogs might be a good way forward.

Unexpectedly, the concentration of the desired parent compounds showed a decreasing trend after prolonged illumination. As proposed by Goswami et al. [32], uncaging of BODIPY analogs in aqueous solutions will yield a BODIPY alcohol next to the desired products. However, this desired alcohol was not easily observed in our uncaging process. Instead, a mass corresponding to a BODIPY-Tris byproduct was detected. We also hypothesized that the photo-bleaching products and/or reactive intermediates of the uncaging process could potentially further react with our desired uncaged compounds under these illumination conditions, thus leading to the decreased concentration of parent compounds.

In conclusion, in the present study we report on the successful BODIPY caging of the H₃R/H₄R agonists immepip and 4-methylhistamine and their evaluation with respect to photo-uncaging and subsequent target engagement. Our results indicate that VUF25657, the caged immepip, is the first successful, caged photopharmacological agent for spatio-temporal control of H₃R function.

4. Materials and Methods

4.1. Chemistry

General information. The raw materials for our experiments were either purchased from commercial suppliers or available in our in-house inventory and used without additional purification. Solvents used in the procedures, such as THF, DCM, DMF, and toluene, were subjected to a purification process through an activated alumina column before use. Experimental procedures were conducted under a N₂ environment unless mentioned otherwise. Thin-layer chromatography (TLC) analyses were employed using Merck F₂₅₄ aluminum-backed silica plates and examined with a 254 nm UV lamp for compound detection. Separation and purification of reaction mixtures were achieved through flash column chromatography, utilizing the Biotage Isolera system. High resolution mass spectrometry analyses were performed on a Bruker microTOF mass spectrometer with electrospray ionization (ESI) in positive-ion mode. Nuclear magnetic resonance (NMR) spectroscopy was conducted on either a Bruker Avance 500 or 600 MHz instrument with a standard temperature (25 °C). The peak multiplicity patterns are categorized as follows: singlet (s), doublet (d), triplet (t), quartet (q), pentet (p), doublet of doublets (dd), doublet of triplets (dt), triplet of doublets (td), broad (br), and multiplet (m). The spectra were internally referenced to the NMR solvent peak at the following chemical shifts: CDCl₃ at 7.26 ppm in ¹H NMR and 77.16 ppm in ¹³C NMR; DMSO-*d*₆ 2.50 ppm in ¹H NMR and 39.52 ppm in ¹³C NMR; and CD₃OD 3.35 ppm in ¹H NMR and 49.00 ppm in ¹³C NMR. Then, 2D NMR HSQC and HMBC techniques were utilized to assign ¹³C signals if needed. IUPAC names were standardized using ChemBioDraw Ultra 19.0. The purity of the synthesized compounds was evaluated as the peak area percentage of the analyzed compound at 254 nm using liquid chromatography-mass spectrometry, which is equipped with a Shimadzu LC-20AD pump and a Shimadzu SPDM20A diode array detector. The mass spectrometry detection was facilitated with a Shimadzu LCMS-2010EV instrument, operating in positive ionization mode. The chromatographic separation was achieved on an Xbridge C18 column (5 μm, 100 mm × 4.6 mm). The following solutions were used as the eluents: solvent A: H₂O with 0.1% HCOOH; and solvent B: MeCN with 0.1% HCOOH. A standard eluent method was used, unless mentioned otherwise: flow rate: 1.0 mL/min, 0–4.5 min, 95–10% A in a linear gradient; 4.5–6.0 min, 10% A; 6.0–6.5 min 10–95% A in a

linear gradient; and 6.5–8.0 min 95% A. Final compounds (**5** and **6**) were >95% pure by HPLC analysis.

4.1.1. (2,8-Diethyl-5,5-difluoro-1,3,7,9-tetramethyl-5H-4 λ^4 ,5 λ^4 -dipyrrolo [1,2-*c*:2',1'-*f*][1,3,2]diazaborinin-10-yl)methyl acetate, **2**

To a solution of 3-ethyl-2,4-dimethyl-1*H*-pyrrole (14.5 mL, 0.107 mol, 2.0 eq) in DCM (642 mL) was added 2-chloro-2-oxoethyl acetate (5.8 mL, 53.7 mmol, 1.0 eq). The mixture was stirred under reflux for 24 h and then cooled to RT. TEA (44.8 mL, 0.332 mol, 6.0 eq) was added followed by the addition of BF₃·O(C₂H₅)₂ (59.7 mL, 0.484 mol, 9.0 eq) and the mixture was stirred at RT for 30 min. The solvent was reduced under vacuum and the dark oily residue was purified by silica gel chromatography with cyclohexane/DCM 30–70% to yield the title compound as a red solid (4.5 g, 22%). ¹H NMR (600 MHz, CDCl₃) δ 5.32 (s, 2H), 2.51 (s, 6H), 2.39 (q, *J* = 7.6 Hz, 4H), 2.25 (s, 6H), 2.14 (s, 3H), 1.05 (t, *J* = 7.6 Hz, 6H). ¹³C NMR (151 MHz, CDCl₃) δ 170.8, 155.2, 136.7, 133.7, 132.4, 131.7, 58.5, 20.8, 17.3, 14.8, 12.8 (t, *J* = 2.8 Hz), 12.7. ¹¹B NMR (160 MHz, CDCl₃) δ 0.60 (t, *J* = 33.0 Hz). ¹⁹F NMR (471 MHz, CDCl₃) δ -145.9 (q, *J* = 32.6 Hz). LC-MS: *t*_R = 5.59 min, purity: 93%, *m/z* [M + H]⁺: 377. Spectral data are in agreement with previous reports [32–34].

4.1.2. (2,8-Diethyl-5,5-difluoro-1,3,7,9-tetramethyl-5H-4 λ^4 ,5 λ^4 -dipyrrolo [1,2-*c*:2',1'-*f*][1,3,2]diazaborinin-10-yl)methanol, **3**

A mixture of 0.10 M aq. NaOH solution (6.3 mL, 0.40 eq) and MeOH (30.0 mL) was stirred for 10 min and then added to a solution of **2** (550 mg, 1.46 mmol, 1.0 eq) in DCM (15.0 mL). The reaction mixture was stirred for 3 h in the dark at RT. The solvents were partially evaporated and the residue was extracted with EtOAc (3 × 30 mL). The combined organic layers were washed with 1 M HCl (2 × 20 mL), brine (20 mL), and dried over anhydrous MgSO₄. The residue was purified by silica gel chromatography with cyclohexane/Et₂O 30–100% to yield the title compound as a red solid (205 mg, 42%). ¹H NMR (500 MHz, CDCl₃) δ 4.93 (s, 2H), 2.50 (s, 6H), 2.44–2.37 (m, 10H), 1.05 (t, *J* = 7.6 Hz, 6H). ¹³C NMR (151 MHz, CDCl₃) δ 154.7, 136.7, 136.5, 133.5, 131.8, 56.3, 17.3, 14.9, 12.78, 12.76. ¹¹B NMR (160 MHz, CDCl₃) δ 0.60 (t, *J* = 33.3 Hz). ¹⁹F NMR (471 MHz, CDCl₃) δ -146.0 (q, *J* = 33.0 Hz). LC-MS: *t*_R = 5.13 min, purity: >99%, *m/z* [M + H]⁺: 335. Spectral data are in agreement with previous reports [33–35].

4.1.3. (2,8-Diethyl-5,5-difluoro-1,3,7,9-tetramethyl-5H-4 λ^4 ,5 λ^4 -dipyrrolo [1,2-*c*:2',1'-*f*][1,3,2]diazaborinin-10-yl)methyl (4-nitrophenyl) carbonate, **4**

To a stirred solution of **3** (1.62 g, 4.83 mmol, 1.0 eq) in PhMe (132 mL) at RT, 4-nitrophenyl chloroformate (3.90 g, 19.3 mmol, 4.0 eq) and pyridine (1.9 mL, 24.2 mmol, 5.0 eq) were added. The reaction mixture was stirred at RT for 3 h. The reaction mixture was washed with satd. aq. NH₄Cl (150 mL) and brine (150 mL). The organic layer was dried over MgSO₄ and solvents were removed under reduced pressure. The residue was purified by gradient reverse phase column with MeCN/H₂O with 0.1% HCOOH from 5–100% to yield the title compound as a red solid (2.10 g, 87%). ¹H NMR (500 MHz, CDCl₃) δ 8.32–8.27 (m, 2H), 7.44–7.37 (m, 2H), 5.59 (s, 3H), 2.53 (s, 6H), 2.41 (q, *J* = 7.6 Hz, 6H), 2.36 (s, 8H), 1.06 (t, *J* = 7.6 Hz, 6H). ¹³C NMR (126 MHz, CDCl₃) δ 155.9, 155.4, 152.4, 145.7, 136.6, 134.1, 132.3, 129.3, 125.5, 121.8, 62.3, 17.3, 14.8, 13.0, 12.9. ¹¹B NMR (160 MHz, CDCl₃) δ 0.59 (t, *J* = 32.9 Hz). ¹⁹F NMR (471 MHz, CDCl₃) δ -143.1 (q, *J* = 32.9 Hz). LC-MS: *t*_R = 5.86 min, purity: 96.6%, *m/z* [M + H]⁺: 500. Spectral data are in agreement with a previous report [35].

4.1.4. (2,8-Diethyl-5,5-difluoro-1,3,7,9-tetramethyl-5H-4 λ^4 ,5 λ^4 -dipyrrolo [1,2-*c*:2',1'-*f*][1,3,2]diazaborinin-10-yl)methyl 4-((1*H*-imidazol-4-yl)methyl)piperidine-1-carboxylate, **5**

To a stirred solution of **4** (0.15 g, 0.30 mmol, 1.0 eq) in THF (4.5 mL) at RT was added 4-((1*H*-imidazol-4-yl)methyl)piperidine·2HBr (0.15 g, 0.45 mmol, 1.5 eq) and DIPEA (0.26 mL,

1.5 mmol, 5.0 eq). The reaction mixture was stirred at RT for 4 h. Upon completion, the reaction mixture was diluted with EtOAc (8.0 mL). The organic phase was washed with satd. aq. NH_4Cl (6.0 mL) and brine (6.0 mL), dried over MgSO_4 , and filtered. Solvents were removed under reduced pressure. The crude product was purified by silica gel chromatography (0–2% MeOH in DCM) to yield the title compound as a red solid (35 mg, 22%). ^1H NMR (600 MHz, $\text{DMSO}-d_6$) δ 11.89–11.62 (m, 1H), 7.47 (s, 1H), 6.82–6.52 (m, 1H), 5.25 (s, 2H), 4.06–3.73 (m, 2H), 2.85–2.70 (m, 2H), 2.46–2.33 (m, 12H), 2.26 (s, 6H), 1.77–1.49 (m, 3H), 1.00 (m, 8H). ^{13}C NMR (151 MHz, CDCl_3) δ 154.9, 154.8, 154.8, 143.8, 137.6, 136.9, 133.9, 133.6, 132.5, 132.4, 116.1, 115.1, 59.0, 44.4, 44.2, 36.0, 35.6, 34.9, 32.6, 32.1, 31.7, 29.8, 17.3, 14.9, 12.8, 12.7, 12.7. Extra peaks were observed, likely as a result of rotamers. ^{11}B NMR (160 MHz, CDCl_3) δ 0.69 (t, $J = 32.3$ Hz). ^{19}F NMR (471 MHz, CDCl_3) δ –145.8 (q, $J = 30.4$ Hz). LC–MS: $t_{\text{R}} = 4.02$ min, purity: >99%, m/z $[\text{M} + \text{H}]^+$: 526. HR–MS: calcd for $\text{C}_{28}\text{H}_{38}\text{BF}_2\text{N}_5\text{O}_2$ $[\text{M} + \text{H}]^+$, 526.3159; found, 526.3185. m.p., 148.7–150.7 °C.

4.1.5. (2,8-Diethyl-5,5-difluoro-1,3,7,9-tetramethyl-5H-4 λ^4 ,5 λ^4 -dipyrrolo [1,2-*c*:2',1'-*f*][1,3,2]diazaborinin-10-yl)methyl (2-(5-methyl-1H-imidazol-4-yl)ethyl)carbamate, 6

To a stirred solution of 4 (0.15 g, 0.30 mmol, 1.0 eq) in dry THF (5.0 mL) at RT was added 2-(5-methyl-1H-imidazol-4-yl)ethan-1-amine·2HCl (89 mg, 0.45 mmol, 1.5 eq) and DIPEA (0.26 mL, 1.5 mmol, 5.0 eq). The reaction mixture was divided into ten aliquots and stirred at that temperature for 4 h. Upon completion, all aliquots were combined and diluted with EtOAc (10.0 mL). The organic phase was washed with satd. aq. NH_4Cl (6.0 mL) and brine (6.0 mL), dried with MgSO_4 and filtered. Solvents were removed under reduced pressure. The crude product was purified by silica gel chromatography (0–1% MeOH in DCM) to yield the title compound as a red solid (95 mg, 55%). ^1H NMR (600 MHz, CD_3OD) δ 7.51 (s, 1H), 5.30 (s, 2H), 3.33 (d, $J = 7.0$ Hz, 2H), 2.76–2.66 (m, 2H), 2.49–2.41 (m, 10H), 2.32 (s, 6H), 2.14 (s, 3H), 1.06 (t, $J = 7.6$ Hz, 6H). ^{13}C NMR (151 MHz, CDCl_3) δ 158.2, 155.7, 138.4, 134.7, 134.3, 134.2, 133.5, 130.1, 127.5, 59.3, 41.9, 26.9, 17.9, 15.1 12.8, 12.7, 10.1. ^{11}B NMR (160 MHz, CDCl_3) δ 0.54 (t, $J = 32.3$ Hz). ^{19}F NMR (471 MHz, CDCl_3) δ –146.5 (q, $J = 32.5$ Hz). LC–MS: $t_{\text{R}} = 3.70$ min, purity: 96.8%, m/z $[\text{M} + \text{H}]^+$: 486. HR–MS: calcd for $\text{C}_{25}\text{H}_{34}\text{BClF}_2\text{N}_4\text{O}_2$ $[\text{M} + \text{H}]^+$, 486.2846; found, 486.2870. m.p., 108.8–116.3 °C.

4.2. Nephelometry

Compounds under investigation were placed into clear, flat-bottom 96-well plates in the absence of light, each containing a distinct concentration (from 10^{-4} M to $10^{-7.5}$ M, with a blank as a baseline reference), and were left to stabilize in a phosphate buffer solution with 1% DMSO for a minimum of 60 min before measurement. A kaolin suspension was placed in each plate at varying concentrations (10^{-4} M to $10^{-7.5}$ M), and was subjected to identical experimental conditions as the test compounds [42]. Utilizing a NEPHELO star Plus instrument from BMG Labtech, Germany, turbidity measurements were taken under a set of parameters: four cycles of readings, initiating the measurement at 0.1 s, with each subsequent reading at 0.1 s interval time. The laser intensity was set to 80%, the beam focus was adjusted to 2.0 mm, and the plates were agitated using an orbital shaking mode at 200 rpm, with an additional 10 s of shaking before the commencement of each cycle. Data analysis was carried out using GraphPad Prism 8 software with the collected data points, generating a line chart that displays both the mean and standard deviation values. These results were compared with the kaolin control to assess the tested compounds.

4.3. (Photo)chemical Stability Assay

Compound aqueous stability and room light stability tests (Figure S2) were carried out with 10 μM samples in 50 mM phosphate buffer plus 1% DMSO at room temperature in clear glass vials. Aqueous stability was checked hourly using LC detection at 254 nm, while room light stability was monitored every 5 min for an hour with identical LC settings.

4.4. Materials for Pharmacological Evaluation

Fetal bovine serum (FBS, #16170078) was obtained from Gibco (Thermo Fisher Scientific, Waltham, MA, USA). Penicillin/streptomycin (P/S) was purchased from GE Healthcare (Uppsala, Sweden). Dulbecco's Modified Eagles Medium (DMEM, #41966-029), Dulbecco's phosphate-buffered saline (DPBS, #15326239), 0.05% Trypsin-EDTA (#11580626), and Hanks' Balanced Salt Solution (HBSS, #11560456) were bought from Thermo Fisher Scientific (Waltham, MA, USA). Linear poly-ethylenimine (PEI, 25-kDa, # 23966-1) was obtained from Polysciences (Warrington, PA, USA). G418 (#108321-42-2) and isoprenaline (#I6504, (R)-3,4-Dihydroxy- α -(isopropylaminomethyl)benzyl alcohol hydrochloride) were purchased from Sigma-Aldrich (St. Louis, MO, USA). Zeocin (#ZEL-43-05) was purchased from InvivoGen (San Diego, CA, USA). Black 96-well plates (#655086) were purchased from Greiner Bio-One (Frickenhausen, Germany). N^{α} -[methyl- ^3H]histamine (#NET1027250UC), [^3H]histamine (#NET732250UC), Microscint-O scintillation liquid (#6013611), GF/C filter plates (#6055690) and MicrobetaWallac Trilux scintillation counter were purchased from PerkinElmer (Groningen, The Netherlands).

4.5. Cell Culture and Transfection

HEK293T cells (ATTC, CRL-1573) were cultured in DMEM supplemented with 10% FBS and 1% P/S in a humidified incubator at 37 °C with 5% CO₂. The HEK293 cell line stably expressing an EPAC-cAMP FRET biosensor was kindly provided by Dr. M. Zimmermann (Interax Biotech, Basal, Switzerland) [43,44]. HEK293-EPAC cells stably co-expressing the H₃R (GenBank accession number NM_007232.3) were generated as previously described [37].

4.6. Membrane Preparation

Membranes were collected from HEK293T cells transiently transfected with H₃R or H₄R by PEI method. In brief, 2 million HEK293T cells were seeded into a 10 cm dish one day before transfection. The next day, the cells were transfected with 2.5 μg cDNA encoding H₃R (GenBank accession number AF140538) or H₄R (GenBank accession number AY136745) supplemented with 2.5 μg empty pcDEF3 [45] plasmid using 20 μg PEI. Two days after transfection, the transfected HEK293T cells were detached using ice-cold PBS, and the membrane pellets were subsequently collected by centrifuging at 1932 \times g at 4 °C for 10 min.

4.7. Radioligand Binding Assay

For competition binding assays, the tested compounds were pre-irradiated to reach the uncaged state. In brief, 0.3 mM stock of photocaged ligand (dissolved in DMSO) was divided into two samples, one of which was subsequently diluted in Tris-HCl buffer (50 mM, pH 7.4) to 3 μM and then irradiated by 560 nm to reach the uncaged state, as confirmed by LC-MS, and the other sample was kept in dark to retain its caged state. The prepared membrane pellets expressing H₃R or H₄R were resuspended in Tris-HCl buffer (50 mM, pH 7.4) and disrupted by 5 s sonication to make membrane suspension. Next, all the following handling was performed under near-infrared light. For testing the binding to H₃R, membrane suspension expressing H₃R was incubated with 2 nM N^{α} -[methyl- ^3H] histamine and increasing concentrations of unlabeled ligands prepared in Tris-HCl buffer. For testing the binding to H₄R, binding assays were performed by displacing 4 nM [^3H] histamine with increasing concentrations of unlabeled ligands prepared in Tris-HCl buffer on membrane suspension expressing H₄R. Following one hour of incubation with continuous shaking at 225 rpm at 25 °C, the reaction was terminated by transferring the mixture to GF/C filter plates that were pre-soaked with a solution containing 0.5% PEI and washed with cold Tris-HCl buffer. After drying for 30 min at 55 °C, the radioactivity remaining on the filters was quantified using a Microbeta Wallac Trilux scintillation counter, following the addition of scintillation liquid with a two-hour delay.

4.8. cAMP Inhibition by FRET-EPAC Biosensor

EPAC-H₃R cells were seeded into black 96-well plates with 50,000 cells per well one day before the experiment. The next day, the culture medium was replaced with HBSS. Subsequently, 10 nM isoprenaline (dissolved in HBSS supplemented with 20 mM thiourea) was added for 10 min incubation to elevate basal cAMP levels. Fluorescence resonance energy transfer (FRET) measurements were recorded by CLARIOstar plate reader in real-time or at 20 min after ligand stimulation.

4.9. Data Analysis

All data are shown as mean \pm S.D. from three individual experiments performed in triplicate. Figures were generated and data analyzed by Prism 9. In radioligand binding assays, the competition binding curves were fitted by 'one-site—Fit K_i' to obtain the equilibrium dissociation constants of unlabeled ligands (K_i) by Cheng-Prusoff equation [46]. In FRET-EPAC assays, the ligand-induced cAMP inhibition was quantified by FRET ratios, dividing the FRET signal at 530 nm by the signal at 480 nm. The response was represented as Δ FRET ratios, obtained by the analysis of 'Fractional difference: (Value—Baseline)/Baseline'. Then the concentration–response curves were fitted using the model: 'log(agonist) vs. response (three parameters)' to obtain potency (pEC₅₀).

5. Conclusions

In conclusion, a BODIPY-based photocaging strategy appears a successful strategy to optically modulate histamine H₃ receptor function. Photocaging of the H₃R agonist immepip leads to **5** (VUF25657), which shows >100-fold lower affinity and potency than immepip. Photo-uncaging of **5** with 560 nm illumination led to the desired parent compound immepip, restoring its binding affinity and potency. These findings prove that **5** is a powerful new photoresponsive tool to modulate H₃R pharmacology, offering promising avenues for future exploration in GPCR photopharmacology efforts.

Supplementary Materials: The following supporting information can be downloaded at: <https://www.mdpi.com/article/10.3390/ph17040536/s1>, Figure S1. Representative plots for nephelometry measurements at different concentrations of parent compounds (immepip and 4-methylhistamine) and caged-compounds **5** and **6** in the dark; Figure S2. Chemical stability of **5** (A/B/C) and **6** (D/E/F) under dark, red light and ambient light; Figure S3. MS calibration curves of the immepip, 4-methylhistamine and BODIPY-caged compounds (**5** and **6**) with their corresponding reference compounds; Figure S4. Photo-uncaging followed by UV–Vis and LC–MS analysis; Figures S5–S31. LC–MS, NMR and HRMS spectroscopy data.

Author Contributions: Conceptualization, Y.Z., M.G., H.F.V., M.W., and R.L.; methodology, Y.Z. and M.G.; data analysis, Y.Z. and M.G.; writing—original draft preparation, Y.Z., M.G., and R.L.; writing—review and editing, H.F.V., M.W., and R.L.; funding acquisition, R.L. All authors have read and agreed to the published version of the manuscript.

Funding: This work was supported by the European Union's Horizon research Human Brain Project (FLAG-ERA JCT2019 HA-CTion). M.G. acknowledges the China Scholarship Council (CSC) for funding (Grant No. 202006310027).

Institutional Review Board Statement: Not applicable.

Informed Consent Statement: Not applicable.

Data Availability Statement: The original contributions presented in the study are included in the article/Supplementary Material, further inquiries can be directed to the corresponding author.

Acknowledgments: Hans Custers and Andrea van de Stolpe are acknowledged for technical assistance. Elwin Janssen is acknowledged for NMR support.

Conflicts of Interest: The authors declare no conflicts of interest.

References

1. Fuchter, M.J. On the Promise of Photopharmacology Using Photoswitches: A Medicinal Chemist's Perspective. *J. Med. Chem.* **2020**, *63*, 11436–11447. [[CrossRef](#)]
2. Silva, J.M.; Silva, E.; Reis, R.L. Light-triggered release of photocaged therapeutics—Where are we now? *J. Control. Release* **2019**, *298*, 154–176. [[CrossRef](#)] [[PubMed](#)]
3. Welleman, I.M.; Hoorens, M.W.H.; Feringa, B.L.; Boersma, H.H.; Szymanski, W. Photoresponsive molecular tools for emerging applications of light in medicine. *Chem. Sci.* **2020**, *11*, 11672–11691. [[CrossRef](#)] [[PubMed](#)]
4. Wijtmans, M.; Josimovic, I.; Vischer, H.F.; Leurs, R. Optical control of Class A G protein-coupled receptors with photoswitchable ligands. *Curr. Opin. Pharmacol.* **2022**, *63*, 102192. [[CrossRef](#)] [[PubMed](#)]
5. Stacko, P.; Solomek, T. Photoremovable Protecting Groups: Across the Light Spectrum to Near-Infrared Absorbing Photocages. *Chimia* **2021**, *75*, 873–881. [[CrossRef](#)] [[PubMed](#)]
6. Bojtár, M.; Németh, K.; Domahidy, F.; Knorr, G.; Verkman, A.; Kállay, M.; Kele, P. Conditionally Activatable Visible-Light Photocages. *J. Am. Chem. Soc.* **2020**, *142*, 15164–15171. [[CrossRef](#)] [[PubMed](#)]
7. Li, Y.; Wang, M.; Wang, F.; Lu, S.; Chen, X. Recent progress in studies of photocages. *Smart Mol.* **2023**, *1*, e20220003. [[CrossRef](#)]
8. Monteiro, D.C.F.; Amoah, E.; Rogers, C.; Pearson, A.R. Using photocaging for fast time-resolved structural biology studies. *Acta Crystallogr. D Struct. Biol.* **2021**, *77*, 1218–1232. [[CrossRef](#)] [[PubMed](#)]
9. Leurs, R.; Vischer, H.F.; Wijtmans, M.; de Esch, I.J. En route to new blockbuster anti-histamines: Surveying the offspring of the expanding histamine receptor family. *Trends Pharmacol. Sci.* **2011**, *32*, 250–257. [[CrossRef](#)] [[PubMed](#)]
10. Panula, P.; Chazot, P.L.; Cowart, M.; Gutzmer, R.; Leurs, R.; Liu, W.L.; Stark, H.; Thurmond, R.L.; Haas, H.L. International Union of Basic and Clinical Pharmacology. XCVIII. Histamine Receptors. *Pharmacol. Rev.* **2015**, *67*, 601–655. [[CrossRef](#)] [[PubMed](#)]
11. Passani, M.B.; Blandina, P. Histamine receptors in the CNS as targets for therapeutic intervention. *Trends Pharmacol. Sci.* **2011**, *32*, 242–249. [[CrossRef](#)] [[PubMed](#)]
12. Ghamari, N.; Zarei, O.; Arias-Montano, J.A.; Reiner, D.; Dastmalchi, S.; Stark, H.; Hamzeh-Mivehroud, M. Histamine H₃ receptor antagonists/inverse agonists: Where do they go? *Pharmacol. Ther.* **2019**, *200*, 69–84. [[CrossRef](#)] [[PubMed](#)]
13. Nieto-Alamilla, G.; Marquez-Gomez, R.; Garcia-Galvez, A.M.; Morales-Figueroa, G.E.; Arias-Montano, J.A. The Histamine H₃ Receptor: Structure, Pharmacology, and Function. *Mol. Pharmacol.* **2016**, *90*, 649–673. [[CrossRef](#)] [[PubMed](#)]
14. Krief, S.; Berrebi-Bertrand, I.; Nagmar, I.; Giret, M.; Belliard, S.; Perrin, D.; Uguen, M.; Robert, P.; Lecomte, J.M.; Schwartz, J.C.; et al. Pitolisant, a wake-promoting agent devoid of psychostimulant properties: Preclinical comparison with amphetamine, modafinil, and solriamfetol. *Pharmacol. Res. Perspect.* **2021**, *9*, e00855. [[CrossRef](#)] [[PubMed](#)]
15. Sarfraz, N.; Okuampa, D.; Hansen, H.; Alvarez, M.; Cornett, E.M.; Kakazu, J.; Kaye, A.M.; Kaye, A.D. pitolisant, a novel histamine-3 receptor competitive antagonist, and inverse agonist, in the treatment of excessive daytime sleepiness in adult patients with narcolepsy. *Health Psychol. Res.* **2022**, *10*, 34222. [[CrossRef](#)] [[PubMed](#)]
16. Wang, J.; Li, X.; Yang, S.; Wang, T.; Xu, Z.; Xu, J.; Gao, H.; Chen, G. Pitolisant versus placebo for excessive daytime sleepiness in narcolepsy and obstructive sleep apnea: A meta-analysis from randomized controlled trials. *Pharmacol. Res.* **2021**, *167*, 105522. [[CrossRef](#)]
17. Schirmer, B.; Neumann, D. The Function of the Histamine H₄ Receptor in Inflammatory and Inflammation-Associated Diseases of the Gut. *Int. J. Mol. Sci.* **2021**, *22*, 6116. [[CrossRef](#)] [[PubMed](#)]
18. Schaper-Gerhardt, K.; Rossbach, K.; Nikolouli, E.; Werfel, T.; Gutzmer, R.; Mommert, S. The role of the histamine H₄ receptor in atopic dermatitis and psoriasis. *Br. J. Pharmacol.* **2020**, *177*, 490–502. [[CrossRef](#)]
19. Shan, L.; Martens, G.J.M.; Swaab, D.F. Histamine-4 Receptor: Emerging Target for the Treatment of Neurological Diseases. *Curr. Top. Behav. Neurosci.* **2022**, *59*, 131–145. [[CrossRef](#)]
20. Lavis, L.D.; Raines, R.T. Bright building blocks for chemical biology. *ACS Chem. Biol.* **2014**, *9*, 855–866. [[CrossRef](#)]
21. Shrestha, P.; Kand, D.; Weinstain, R.; Winter, A.H. meso-Methyl BODIPY Photocages: Mechanisms, Photochemical Properties, and Applications. *J. Am. Chem. Soc.* **2023**, *145*, 17497–17514. [[CrossRef](#)] [[PubMed](#)]
22. Lim, H.D.; van Rijn, R.M.; Ling, P.; Bakker, R.A.; Thurmond, R.L.; Leurs, R. Evaluation of histamine H₁-, H₂-, and H₃-receptor ligands at the human histamine H₄ receptor: Identification of 4-methylhistamine as the first potent and selective H₄ receptor agonist. *J. Pharmacol. Exp. Ther.* **2005**, *314*, 1310–1321. [[CrossRef](#)]
23. Vollinga, R.C.; de Koning, J.P.; Jansen, F.P.; Leurs, R.; Menge, W.M.; Timmerman, H. A new potent and selective histamine H₃ receptor agonist, 4-(1H-imidazol-4-ylmethyl)piperidine. *J. Med. Chem.* **1994**, *37*, 332–333. [[CrossRef](#)]
24. Kitbunnadaj, R.; Hashimoto, T.; Poli, E.; Zuiderveld, O.P.; Menozzi, A.; Hidaka, R.; de Esch, I.J.; Bakker, R.A.; Menge, W.M.; Yamatodani, A.; et al. N-substituted piperidinyl alkyl imidazoles: Discovery of methimepip as a potent and selective histamine H₃ receptor agonist. *J. Med. Chem.* **2005**, *48*, 2100–2107. [[CrossRef](#)]
25. Ishikawa, M.; Furuuchi, T.; Yamauchi, M.; Yokoyama, F.; Kakui, N.; Sato, Y. Synthesis and structure-activity relationships of N-aryl-piperidine derivatives as potent (partial) agonists for human histamine H₃ receptor. *Bioorg. Med. Chem.* **2010**, *18*, 5441–5448. [[CrossRef](#)] [[PubMed](#)]
26. Vaccaro, W.D.; Sher, R.; Berlin, M.; Shih, N.Y.; Aslanian, R.; Schwerdt, J.H.; McCormick, K.D.; Piwinski, J.J.; West, R.E., Jr.; Anthes, J.C.; et al. Novel histamine H₃ receptor antagonists based on the 4-[(1H-imidazol-4-yl)methyl]piperidine scaffold. *Bioorg. Med. Chem. Lett.* **2006**, *16*, 395–399. [[CrossRef](#)]

27. Im, D.; Kishikawa, J.I.; Shiimura, Y.; Hisano, H.; Ito, A.; Fujita-Fujiharu, Y.; Sugita, Y.; Noda, T.; Kato, T.; Asada, H.; et al. Structural insights into the agonists binding and receptor selectivity of human histamine H₄ receptor. *Nat. Commun.* **2023**, *14*, 6538. [[CrossRef](#)]
28. Xia, R.; Shi, S.; Xu, Z.; Vischer, H.F.; Windhorst, A.D.; Qian, Y.; Duan, Y.; Liang, J.; Chen, K.; Zhang, A.; et al. Structural basis of ligand recognition and design of antihistamines targeting histamine H₄ receptor. *Nat. Commun.* **2024**, *15*, 2493. [[CrossRef](#)] [[PubMed](#)]
29. Bardhan, A.; Deiters, A. Development of photolabile protecting groups and their application to the optochemical control of cell signaling. *Curr. Opin. Struct. Biol.* **2019**, *57*, 164–175. [[CrossRef](#)]
30. Ellis-Davies, G.C.R. Useful Caged Compounds for Cell Physiology. *Acc. Chem. Res.* **2020**, *53*, 1593–1604. [[CrossRef](#)]
31. Jia, S.; Sletten, E.M. Spatiotemporal Control of Biology: Synthetic Photochemistry Toolbox with Far-Red and Near-Infrared Light. *ACS Chem. Biol.* **2022**, *17*, 3255–3269. [[CrossRef](#)] [[PubMed](#)]
32. Goswami, P.P.; Syed, A.; Beck, C.L.; Albright, T.R.; Mahoney, K.M.; Unash, R.; Smith, E.A.; Winter, A.H. BODIPY-derived photoremovable protecting groups unmasked with green light. *J. Am. Chem. Soc.* **2015**, *137*, 3783–3786. [[CrossRef](#)] [[PubMed](#)]
33. Amat-Guerri, F.; Liras, M.; Carrascoso, M.L.; Sastre, R. Methacrylate-tethered analogs of the laser dye PM567--synthesis, copolymerization with methyl methacrylate and photostability of the copolymers. *Photochem. Photobiol.* **2003**, *77*, 577–584. [[CrossRef](#)] [[PubMed](#)]
34. Ma, J.; Egodawaththa, N.M.; Guruge, C.; Marquez, O.A.V.; Likes, M.; Nesnas, N. Blue and Green Light Responsive Caged Glutamate. *J. Photochem. Photobiol. A Chem.* **2024**, *447*, 115183. [[CrossRef](#)]
35. Rubinstein, N.; Liu, P.; Miller, E.W.; Weinstain, R. meso-Methylhydroxy BODIPY: A scaffold for photo-labile protecting groups. *Chem. Commun.* **2015**, *51*, 6369–6372. [[CrossRef](#)] [[PubMed](#)]
36. Mocking, T.A.M.; Verweij, E.W.E.; Vischer, H.F.; Leurs, R. Homogeneous, Real-Time NanoBRET Binding Assays for the Histamine H₃ and H₄ Receptors on Living Cells. *Mol. Pharmacol.* **2018**, *94*, 1371–1381. [[CrossRef](#)] [[PubMed](#)]
37. Gao, M.; Dekker, M.E.; Leurs, R.; Vischer, H.F. Pharmacological characterization of seven human histamine H₃ receptor isoforms. *Eur. J. Pharmacol.* **2024**, *968*, 176450. [[CrossRef](#)] [[PubMed](#)]
38. Kaplan, J.H.; Forbush, B., 3rd; Hoffman, J.F. Rapid photolytic release of adenosine 5'-triphosphate from a protected analogue: Utilization by the Na:K pump of human red blood cell ghosts. *Biochemistry* **1978**, *17*, 1929–1935. [[CrossRef](#)] [[PubMed](#)]
39. Xiong, H.; Xu, Y.; Kim, B.; Rha, H.; Zhang, B.; Li, M.; Yang, G.-F.; Kim, J.S. Photo-controllable biochemistry: Exploiting the photocages in phototherapeutic window. *Chem* **2023**, *9*, 29–64. [[CrossRef](#)]
40. Klan, P.; Solomek, T.; Bochet, C.G.; Blanc, A.; Givens, R.; Rubina, M.; Popik, V.; Kostikov, A.; Wirz, J. Photoremovable protecting groups in chemistry and biology: Reaction mechanisms and efficacy. *Chem. Rev.* **2013**, *113*, 119–191. [[CrossRef](#)]
41. Kand, D.; Liu, P.; Navarro, M.X.; Fischer, L.J.; Rousso-Noori, L.; Friedmann-Morvinski, D.; Winter, A.H.; Miller, E.W.; Weinstain, R. Water-Soluble BODIPY Photocages with Tunable Cellular Localization. *J. Am. Chem. Soc.* **2020**, *142*, 4970–4974. [[CrossRef](#)] [[PubMed](#)]
42. Roessler, W.G.; Brewer, C.R. Permanent turbidity standards. *Appl. Microbiol.* **1967**, *15*, 1114–1121. [[CrossRef](#)] [[PubMed](#)]
43. Mathiesen, J.M.; Vedel, L.; Brauner-Osborne, H. cAMP biosensors applied in molecular pharmacological studies of G protein-coupled receptors. *Methods Enzymol.* **2013**, *522*, 191–207. [[CrossRef](#)] [[PubMed](#)]
44. Scharf, M.M.; Zimmermann, M.; Wilhelm, F.; Stroe, R.; Waldhoer, M.; Kolb, P. A Focus on Unusual ECL2 Interactions Yields β_2 -Adrenergic Receptor Antagonists with Unprecedented Scaffolds. *ChemMedChem* **2020**, *15*, 882–890. [[CrossRef](#)] [[PubMed](#)]
45. Goldman, L.A.; Cutrone, E.C.; Kotenko, S.V.; Krause, C.D.; Langer, J.A. Modifications of vectors pEF-BOS, pcDNA1 and pcDNA3 result in improved convenience and expression. *Biotechniques* **1996**, *21*, 1013–1015. [[CrossRef](#)]
46. Cheng, Y.; Prusoff, W.H. Relationship between the inhibition constant (K_i) and the concentration of inhibitor which causes 50 per cent inhibition (IC_{50}) of an enzymatic reaction. *Biochem. Pharmacol.* **1973**, *22*, 3099–3108. [[CrossRef](#)]

Disclaimer/Publisher's Note: The statements, opinions and data contained in all publications are solely those of the individual author(s) and contributor(s) and not of MDPI and/or the editor(s). MDPI and/or the editor(s) disclaim responsibility for any injury to people or property resulting from any ideas, methods, instructions or products referred to in the content.